Available on CMS information server

**CMS NOTE 1997/030**

The Compact Muon Solenoid Experiment

# CMS Note

Mailing address: CMS CERN, CH-1211 GENEVA 23, Switzerland

**7 May 1997**

# APD properties and recovery from radiation damage

S. Baccaro[1], B. Borgia[2], S. Caruso[1], F. Cavallari[2], I. Dafinei[2], M. Diemoz[2], I. Emeliantchik[3], A. Festinesi[1], E. Longo[2], M. Montecchi[1], G. Organtini[4], G. Rosi[1]

INFN - Sezione di Roma, Roma, Italy

1 ENEA-INN/TEC Casaccia Research Center, Roma, Italy
2 Department of Physics, Università ”La Sapienza”, Roma, Italy
3 Bielorussian State University, Minsk, Bielorussia
4 Department of Physics, Università ”Roma-TRE”, Roma, Italy

**Abstract**

Avalanche photodiodes will be used to detect scintillation light from $PbWO_4$ crystals in the CMS electromagnetic calorimeter. Properties of Hamamatsu APD are reported and special attention has been devoted to the study of radiation hardness and room temperature annealing. We found a fast recovery with a time constant of 1.3 days, a medium fast recovery with $\tau$ of the order of 10 days and indication of a third component with very long time constant of the order of 300 days.

| APD (batch B) T≃18°C (summer 1996) | | | | | |
|---|---|---|---|---|---|
| APD | C(pF) | Front Window | V(V) | $I_D$(nA) | Area ($cm^2$) |
| BA | 120÷130 | $SiO_2$ | 193 | 20 | .2 |
| BC | 130÷140 | $SiO_2$ | 182 | 2 | .2 |
| BD | 420÷430 | $SiO_2$ | 119 | 2.5 | .2 |
| BE | 470÷480 | $SiO_2$ | 113 | 10 | .2 |
| BA-N | 120÷130 | $Si_3N_4$ | 193 | 2 | .2 |

Table 1
Parameters of the new APD's from Hamamatsu : capacitance, front window layer, bias for a gain of 50, dark current for a gain of 50, area.

## 1. Introduction

Avalanche Photodiodes were proposed as photon detectors for the CMS electromagnetic calorimeter, made of $PbWO_4$ crystals [1]. The low light yield of these crystals and the high magnetic field of the experiment require a detector with high quantum efficiency, some internal amplification and not sensitive to magnetic fields. Furthermore LHC is a hard environment for what concerns the radiation levels in the detectors, so the radiation resistance is mandatory for the APD's.

In the framework of the common R&D program with Hamamatsu, the properties of a batch of APD's (named batch B) delivered in summer 96 and developed to improve the radiation resistance are investigated. The structural characteristics of these devices are summarized in Table 1.

One sample for each type BA BD BE were measured and irradiated and three samples for type BC which was chosen by the collaboration to compare the results coming from different laboratories.

If not otherwise stated, all the measurements refer to a temperature T= $18^{\circ}$C.

## 2. APD characterization

Relevant APD parameters are the gain M that can be reached well within operating conditions, the quantum efficiency $\varepsilon_{\mathrm{Q}}$, the excess noise factor F (which affect the stochastic term of the energy resolution) and the electronic noise induced by the device. The characteristics of the APD which influence the electronic noise are the dark current ($\mathrm{I_D}$) and the capacitance ($\mathrm{C_D}$). The dark current can be divided in a bulk ($\mathrm{I_B}$) and a surface ($\mathrm{I_S}$) term. Neglecting the small contribution due to holes, the effective dark current is given by:

$$\mathrm{I_D} = \mathrm{I_B} \cdot \mathrm{M} + \mathrm{I_S}. \tag{1}$$

The equivalent energy electronic noise[1)] in the APD's with a charge preamplifier and a RC-CR shaper with shaping time $\tau$ and capacitance $\mathrm{C_{PA}}$ is given by two terms, a parallel noise term and a series noise term [2]:

$$\begin{aligned} \frac{\sigma_{\mathrm{par}}(\mathrm{MeV})}{\mathrm{E}} &\approx e\frac{\sqrt{2\mathrm{q}(\mathrm{I_S}+\mathrm{FM^2I_B})}\sqrt{\tau}}{\mathrm{q}\sqrt{8}\mathrm{N_{pe}ME}} \\ \frac{\sigma_{\mathrm{ser}}(\mathrm{MeV})}{\mathrm{E}} &\approx e\frac{(\mathrm{C_D}+\mathrm{C_{PA}})}{\mathrm{q}\sqrt{8}\sqrt{\tau}\mathrm{N_{pe}ME}}\sqrt{4\mathrm{KT}\left(\mathrm{R_S}\left(\frac{\mathrm{C_D}}{\mathrm{M}}\right)^2+\frac{0.7}{\mathrm{g_m}}\right)} \end{aligned} \tag{2}$$

where $\mathrm{R_S}$ is the series resistance of the APD, $\mathrm{g_m}$ is the transconductance of the amplifier transistor, $\mathrm{N_{pe}}$ is the number of photoelectrons per MeV yielded by the crystals coupled to the APD and E is the particle energy in MeV.

## 3. Measurements

The APD's were measured several times before and after irradiation. The dark current was measured with the picoamperometers Keithley 486 or 487. The bias to the APD was provided either by the Keithley 487 itself or by

[1)] We define equivalent energy electronic noise the fluctuations induced by purely electronic noise of the APD when it is detecting light emitted by a scintillating crystal hit by a particle dissipating energy E.

a Fluke 415B high voltage source.

Because the characteristics of the APD's are very sensitive to temperature changes, it is crucial to have a good temperature stability and control. The temperature monitoring was done with temperature sensors whose accuracy is 0.1$^{o}$C, but the environment conditions do not allow a stability of the effective temperature of the APD to more than 0.5$^{o}$C. This fact induces an error on the dark current of the order of a few percent.

### 3.1. Gain

The gain of an APD can be easily measured by continuous light method: the dark current and the current under continuous illumination are recorded for each bias voltage. The gain is then calculated as the current amplification with respect to a bias of 10 V, where no amplification is assumed:

$$\mathrm{M} = \frac{\mathrm{I_{ill}(V_{bias}) - I_D(V_{bias})}}{\mathrm{I_{ill}(10\ V) - I_D(10\ V)}}. \tag{3}$$

A blue LED was used as light source. The APD was kept in a dark box on a special support and the light was fetched to the APD through an optic fiber. This configuration allows a very stable setup. In Figure 1 the gain versus the reverse bias voltage is plotted for Hamamatsu BA and BD prototypes.

High stability in the voltage and small temperature dependence of the gain are required for stable operating conditions in CMS. In Figure 2 we have plotted the voltage dependence of the gain for Hamamatsu BA-N prototype. For a gain of 50, $\frac{1}{\mathrm{M}}\frac{\mathrm{dM}}{\mathrm{dV}}$ is about 5%. A discussion of the temperature dependence of the gain is done in Section 4.2.

### 3.2. Dark current

From the measurement of dark current and gain it is possible to disentangle the contributions of the bulk and surface currents:

$$\frac{\mathrm{I_D}}{\mathrm{M}} = \frac{\mathrm{I_S}}{\mathrm{M}} + \mathrm{I_B} \tag{4}$$

In Figure 3, the two contributions are fitted for the BA and BA-N prototypes. It must be emphasized that in the parallel noise term (Eq. (2)), the bulk current is multiplied by $\mathrm{M}^2$: for high gain, the other contributions can often be neglected. In this respect the noise is especially low for the Hamamatsu prototype with the $\mathrm{Si_3N_4}$ window (prototype BA-N), see Figure 3(b).

### 3.3. Quantum efficiency

The measurement of the quantum efficiency was performed with the setup of Figure 4. A Xe lamp followed by a mechanical chopper and a monochromator was used as light source. The modulated signal resulting from the APD was measured with a lock-in amplifier. The APD quantum efficiency was calculated from the ratio of the signal of the APD at 10 V and the signal of a calibrated PIN diode exposed in the same conditions, multiplied by its quantum efficiency:

$$\varepsilon_{\mathrm{Q}} = \frac{\mathrm{signal\ APD(10V)}}{\mathrm{signal\ PIN}} \cdot \varepsilon_{\mathrm{Q}}^{\mathrm{PIN}}. \tag{5}$$

Figure 5(a) shows the dependence of the quantum efficiency on the wavelenght for the APD BA-N and BC. There is a significant difference between the quantum efficiency of the APD type BA-N with the front window of silicon nitride and the BC type with silicon oxide. This difference is mainly due to the respective refractive index that is 1.5 for $\mathrm{SiO_2}$ and $\sim 2$ for $\mathrm{Si_3N_4}$, which determines a difference in reflectance [3].

## 4. Temperature effects

### 4.1. Temperature dependence of the dark current

Before irradiation the bulk current is due to the thermal generation of carriers and the temperature dependence can be described by [4]:

$$\mathrm{I_B} \propto \mathrm{T}^{3/2} \cdot \mathrm{e}^{-\mathcal{E}_{\mathrm{G}}/2\mathrm{KT}} \tag{6}$$

where $\mathcal{E}_{\mathrm{G}}$ is the energy of the forbidden gap in silicon, which is about 1.2 eV.

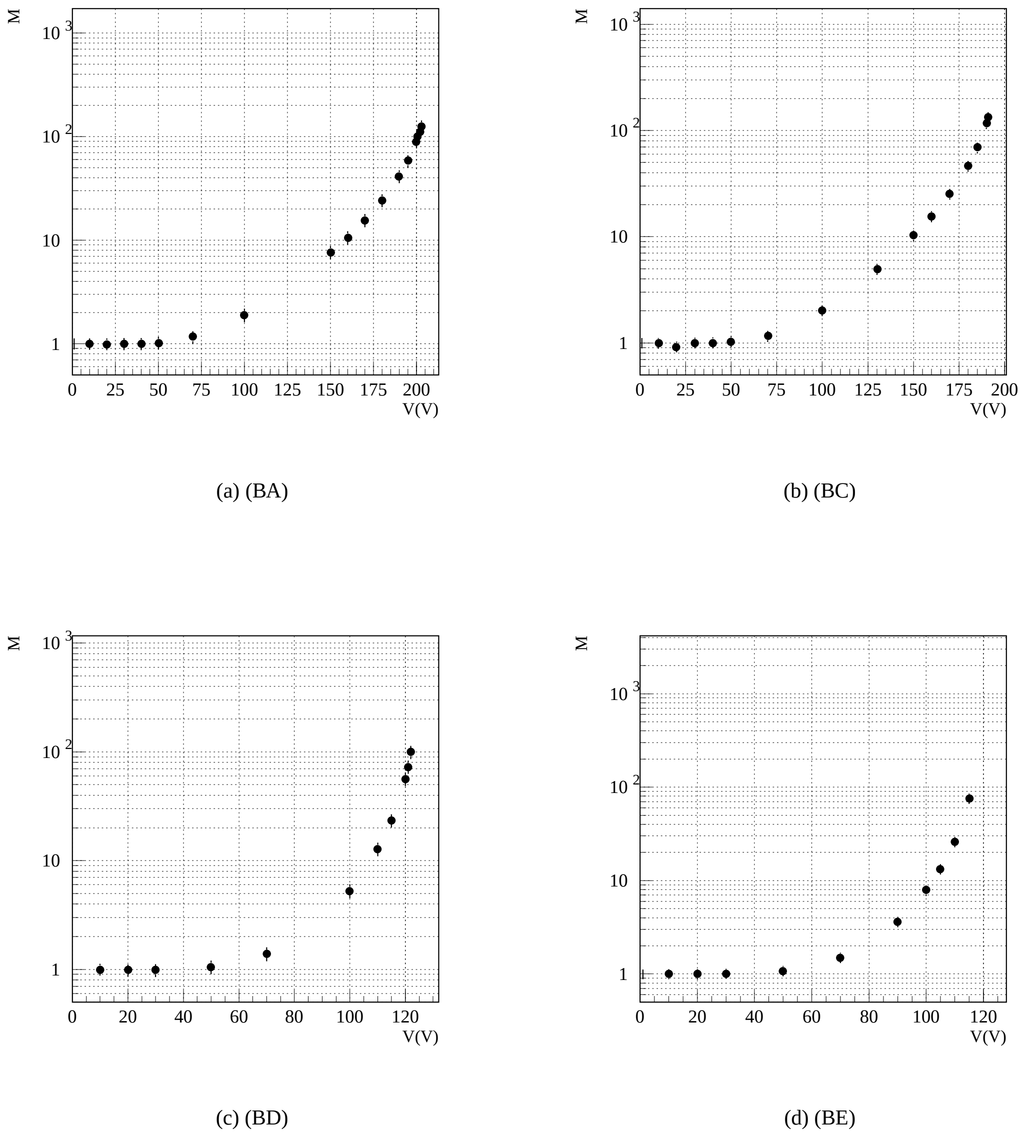


Figure 1. Gain versus bias voltage for the APD prototype BA BC BD and BE of Hamamatsu.

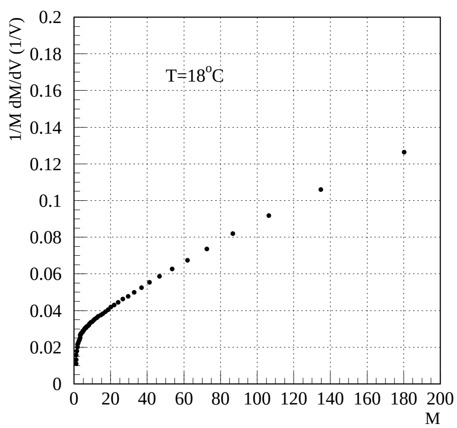


Figure 2. Voltage dependence of the gain for the APD prototype BA-N of Hamamatsu.

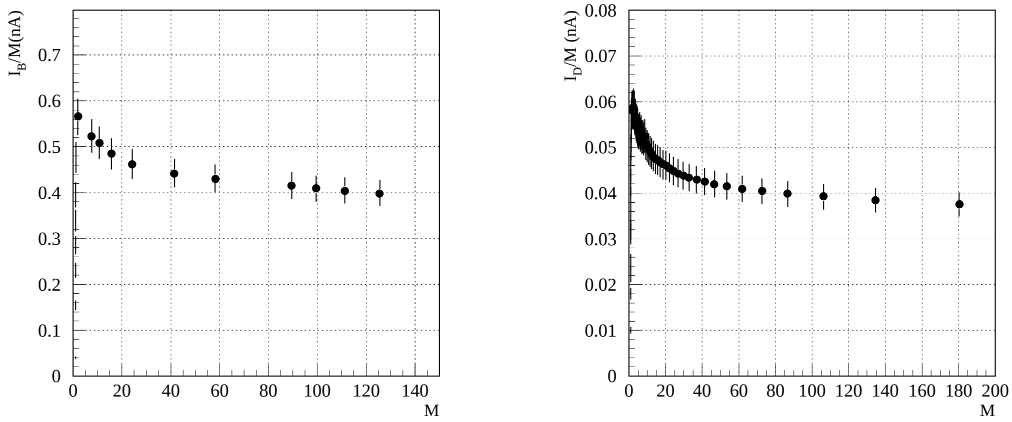


(a) (BA)

(b) (BA-N)

Figure 3. Dark current divided by gain versus gain for the APD prototype BA and BA-N of Hamamatsu at 18°C. The gain was measured with continuous light with a blue and green led.

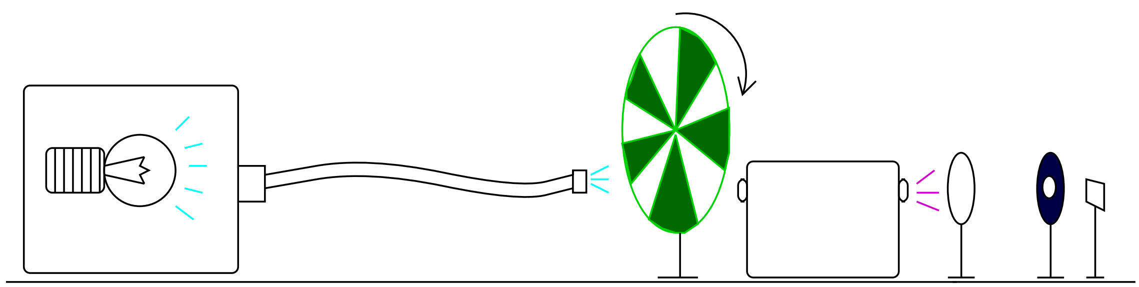

(a) (b) (c) (d) (e) (f) (g)

Figure 4. Setup for the measurement of the quantum efficiency.
(a) Xenon lamp
(b) Fiber optic
(c) Chopper
(d) Monochromator
(e) Lens
(f) Iris diaphragm
(g) APD support

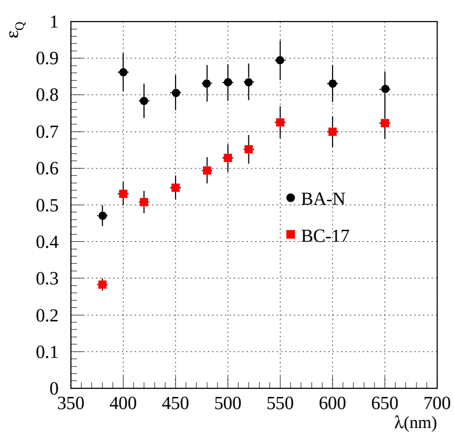


Figure 5. Quantum efficiency of the APD type BA-N and BC. The measurements were done at 24°C.

The surface current should have two contributions: a resistive term and a term similar to the bulk current, without amplification. Figure 6(a) shows the dark current divided by the gain at different temperatures for the APD BA-N. Figure 6(b) shows the contributions of the bulk and surface currents. From the fit to the bulk current a value $\mathcal{E}_G = (1.15{\pm}0.09)$ eV is found. In this device the surface current has a linear behaviour with respect to temperature and so it can be regarded as purely resistive.

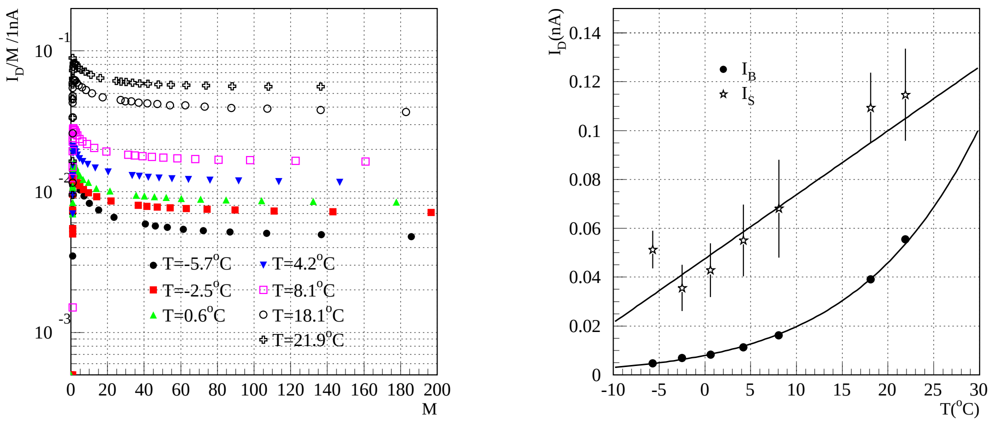


(a) (b)

Figure 6. (a) Dark current divided by gain at different temperatures for the APD BA-N.
(b) Bulk and surface current as a function of temperature. The fit to the bulk current was performed using Eq. (6) while the surface current can be described by a linear fit.

### 4.2. Temperature dependence of the gain

Figure 7(a) shows the gain as a function of bias voltage at different temperatures. The gain of an APD decreases with increasing temperature. For these devices the avalanche region is usually described by the formula [4]:

$$\mathrm{M(V)} = \frac{1}{1 - (\mathrm{V}/\mathrm{V_b})^{\mathrm{n}}} \tag{7}$$

where $\mathrm{V_b}$ is the breakdown voltage and n is a coefficient to be determined experimentally. Both $\mathrm{V_b}$ and n depend on the temperature and this dependence is linear to a first approximation. Usually the temperature dependence of the gain around the working point M=50 at T=18°C is given as the coefficient $1/\mathrm{M}(\mathrm{dM}/\mathrm{dT})$ (shown in Figure 7(b)) which corresponds to:

$$\frac{1}{\mathrm{M}}\frac{\mathrm{dM}}{\mathrm{dT}} = \frac{1}{\mathrm{M}}\frac{\partial \mathrm{M}}{\partial \mathrm{V_b}}\frac{\partial \mathrm{V_b}}{\partial \mathrm{T}} + \frac{1}{\mathrm{M}}\frac{\partial \mathrm{M}}{\partial \mathrm{n}}\frac{\partial \mathrm{n}}{\partial \mathrm{T}} = -\mathrm{M}\left(\frac{\mathrm{V}}{\mathrm{V_b}}\right)^{\mathrm{n}}\left[\frac{\mathrm{n}}{\mathrm{V_b}}\frac{\partial \mathrm{V_b}}{\partial \mathrm{T}} + \ln\left(\frac{\mathrm{V_b}}{\mathrm{V}}\right)\frac{\partial \mathrm{n}}{\partial \mathrm{T}}\right]. \tag{8}$$

Figure 8(a) and (b) report the temperature dependence of n and $\mathrm{V_b}$ for APD BA-N type. The coefficient $1/\mathrm{M}(\mathrm{dM}/\mathrm{dT})$ has similar values for all these APD's.

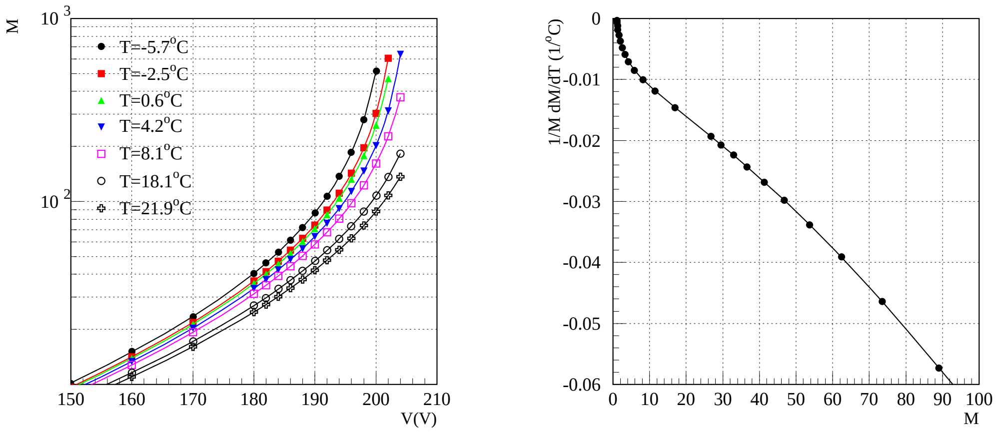


(a) (b)

Figure 7. Gain curves at different temperatures (a) and (b) temperature coefficient of the gain for the APD prototype BA-N of Hamamatsu.

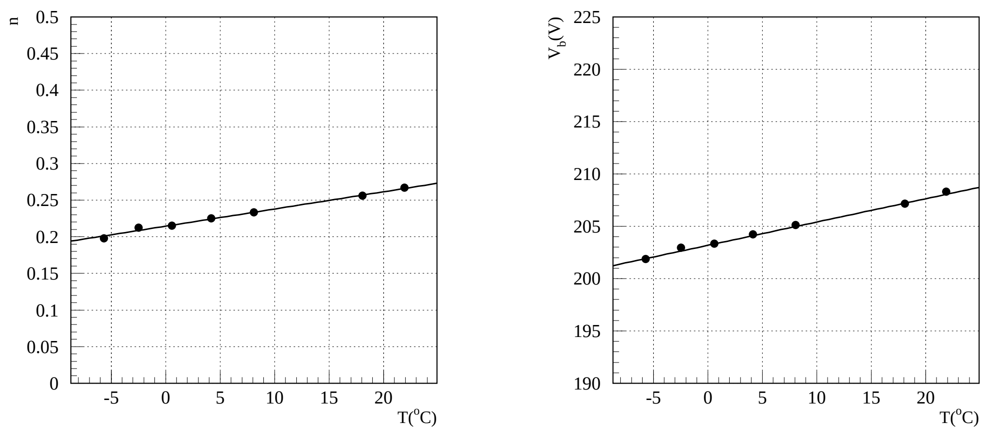


(a) (b)

Figure 8. Temperature dependence of n and $V_b$ for the APD prototype BA-N of Hamamatsu.

# 5. Radiation damage

## 5.1. Introduction

Many groups (see for example [5] and [6]) studied radiation damage in silicon devices. In principle the structure of an APD is significantly different from commercial diodes used in these investigations, nevertheless the results of these studies can be taken as a starting point. The damage in diodes occurs through two mechanisms:

- the bulk damage, due to displacement of atoms from their lattice sites, causes an increase in the dark current. It depends on the Non Ionizing Energy Loss (NIEL) of the radiation in the medium [7], varying on the particle type and energy[2)].
- the surface damage, which causes defects on the front layer and leads to an increase in the surface current.

The doses of $\gamma$ and neutrons in CMS corresponding to 10 years of LHC running was calculated in [1]. In the ECAL barrel region the upper limit on the neutron dose was estimated to be $2{\cdot}10^{13}$neutrons/cm$^2$ with an energy spectrum around 1 MeV, while the $\gamma$ dose will be around 0.3÷0.5 Mrad. At these doses the bulk damage caused by neutrons will be the dominant effect.

The main consequence of neutron damage is the creation of defects in the silicon lattice like vacancies and displacements of atoms (these can be isolated point defects or more complex defects, like clusters). Due to these defects, new energy levels are allowed for the electrons and holes in the forbidden gap of the semiconductor. By some experimental techniques like TSC and DLTS it is possible to measure the energy of these radiation-induced levels. Some of these levels were classified and the corresponding defects were identified [6].

Due to the presence of the defects, there is an additional dark current $\mathrm{I_D^{irr}}$ which increases linearly with the concentration of the defects and thus linearly with the neutron administered dose $\Phi$:

$$\mathrm{I_D^{irr}} = \alpha \cdot \mathrm{V} \cdot \Phi \tag{9}$$

where V is the volume of the device. This linear behaviour is valid until a few $10^{13}$ neutrons/cm$^2$. A compilation of the values of $\alpha$, mainly measured on diodes, can be found in [8]. This parameter depends on the incident particle, on the temperature and on the time elapsed from the irradiation.

In fact the measurements show that the dark current induced by the radiation damage tends to recover with a law which is a sum of exponentials, each defect being characterized by its proper recovery time $\tau_\mathrm{i}$:

$$\mathrm{I_D^{irr}(t)} = \mathrm{I_D^{irr}}(0) \cdot \sum_\mathrm{i} \mathrm{g_i} \cdot \mathrm{e}^{-\mathrm{t}/\tau_\mathrm{i}}. \tag{10}$$

The measured weights $\mathrm{g_i}$ of each component are given in Table 2. In [9] a detailed study of the time dependence

| $g_i$ | $\tau_i$ |
|---|---|
| 0.2 | 12.9 min |
| 0.3 | 85.4 min |
| 0.13 | 30.5 hours |
| 0.13 | 6.6 days |
| 0.24 | $\infty$ |

Table 2
Recovery components measured on commercial diodes [5].

of the recovery on diodes was done. From this study one can deduce a value for $\alpha$ in Eq. (9) at 18°C and after 2 days from the irradiation of about $8{\cdot}10^{-17}$A/cm.

The temperature dependence of the dark current after irradiation is given by [5]:

$$\mathrm{I_D^{irr}} \propto \mathrm{T}^2 \cdot \mathrm{e}^{-(\mathcal{E}_\mathrm{T}/\mathrm{KT})} \tag{11}$$

in a model where the dark current is generated by a single type of trap with energy $\mathcal{E}_\mathrm{T}$.

2) For the comparisons 1 MeV neutrons are taken as a reference.

### 5.2. Experimental results

In this study the APD's were irradiated at the Tapiro reactor [10] at Enea-Casaccia. The energy spectrum of the neutrons in this facility is plotted in Figure 9. Because it is peaked at about 1 MeV, it can well simulate the LHC environment. Together with the neutrons there is a gamma background corresponding to 175 rad for a dose of $10^{12}$n/cm$^2$.

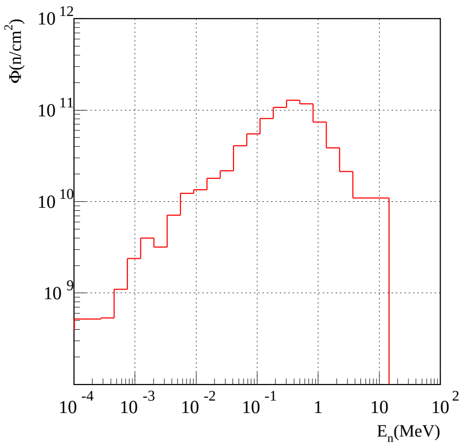


Figure 9. Energy spectrum of the TAPIRO reactor (ENEA-Casaccia).

The APD's, kept under a bias corresponding to a gain of 50, were irradiated in 6 steps, up to the final dose of about $4{\cdot}10^{13}$neutrons/cm$^2$, as reported in Table 3.

The irradiation in this facility takes about 20 to 30 minutes. The APD's were measured about 2 to 5 days after the irradiation (see Table 4), to allow for the deactivation of the gold contacts and the silicon itself. The whole procedure took about 1 month.

Figure 10 shows the bulk current versus neutron dose for prototype BA5. In the same picture these results are compared with those on the same APD type obtained in other irradiation facilities (PSI and RAL). For this comparison the PSI proton dose was multiplied by the proper NIEL factor [7] to be compared to 1 MeV neutrons. All of the measurements were rescaled at a reference temperature of 18$^o$C, as explained in Section 5.5. Moreover all the data were corrected for the recovery due to the long time which was needed to irradiate the APD's up to the final dose and to the fact that the measurements in the various laboratories were done at different time after the irradiation. The correction for the recovery is based on Eq. (10), as explained in Table 5 caption. After these corrections, there is good agreement between measurements performed in the various laboratories.

Since this batch of APD's from Hamamatsu was especially developed to improve the radiation hardness, it is very interesting to compare their behaviour with the old ones. The results from the RAL neutron irradiation of an old APD (Hamamatsu S5345) are also shown. From this Figure one can clearly see that there is a big improvement in the radiation hardness of these devices.

The increase in the bulk current appears to be linear with respect to the neutron dose $\Phi$, as for other silicon devices described in the literature (see Eq. (9)). In Eq. (9), it is reasonable to assume that [11] the volume is given by the area of the APD times the effective thickness $\mathrm{d_{eff}}$. Measurements of the effective thickness for these diodes give values of about 5$\mu$m. Figure 10 shows a comparison of the experimental results with the prediction for a diode of 5$\mu$m thickness and $\alpha$=$8{\cdot}10^{-17}$A/cm.

Furthermore, assuming $\mathrm{d_{eff}}$ =5$\mu$m, the values of $\alpha$ in Table 6 can be estimated. In the evaluation of these parameters, the data from Table 5 were used.

APD's of type BC were chosen by the collaboration to compare the results on radiation damage. Three diodes of this type were irradiated with different doses. The values of $\alpha$ estimated for these devices are written in Table 6. The results are consistent among each other and with similar measurements done in the other laboratories.

| | Dose given for each step | | | | | |
|---|---|---|---|---|---|---|
| $\Phi(10^{11}\mathrm{n/cm^2})$ | 1.9 | 5.7 | 18.5 | 56.7 | 184 | 375 |

Table 3
Integrated dose reached at each of the 6 steps of irradiation.

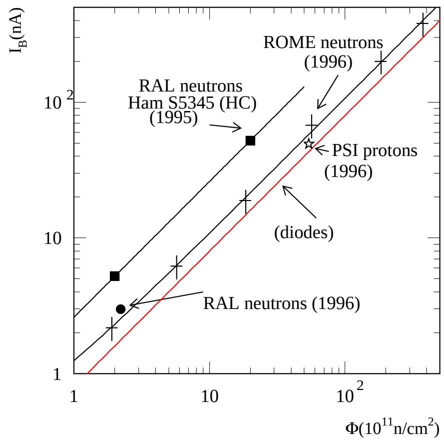


Figure 10. Irradiation induced bulk current versus neutron dose. The current is extrapolated to 2 days after the irradiation (see Table 5) and is measured at 18°C. The straight line marked *diodes*is computed by Eq. (9) using $\mathrm{d_{eff}} = 5\mu\mathrm{m}$ and $\alpha = 8 \cdot 10^{-17}$A/cm.

| | $\Phi_1$ | | $\Phi_2$ | | $\Phi_3$ | | $\Phi_4$ | | $\Phi_5$ | | $\Phi_6$ | |
|---|---|---|---|---|---|---|---|---|---|---|---|---|
| | $\mathrm{d_{irr}}$ | $\Delta\mathrm{d_m}$ | $\mathrm{d_{irr}}$ | $\Delta\mathrm{d_m}$ | $\mathrm{d_{irr}}$ | $\Delta\mathrm{d_m}$ | $\mathrm{d_{irr}}$ | $\Delta\mathrm{d_m}$ | $\mathrm{d_{irr}}$ | $\Delta\mathrm{d_m}$ | $\mathrm{d_{irr}}$ | $\Delta\mathrm{d_m}$ |
| BA5 | 0 | 2 | 4 | 6 | 11 | 5 | 18 | 6 | 28 | 2 | 32 | 6 |
| BC5 | 0 | 2 | 4 | 6 | 11 | 5 | 21 | 3 | 28 | 3 | 35 | 3 |
| BD5 | 0 | 2 | 4 | 6 | 11 | 5 | 21 | 3 | 28 | 3 | 35 | 3 |
| BE5 | 0 | 2 | 4 | 6 | 11 | 5 | 21 | 3 | 28 | 3 | 36 | 2 |

Table 4
The table gives, for each APD, the day $\mathrm{d_{irr}}$ when every irradiation occurred, with respect to the first irradiation (day 0). The table shows also the time interval $\Delta\mathrm{d_m}$ elapsed between each irradiation and the measurement of the current $\mathrm{I_B}$ in Table 5.

| APD | not irr. | $\Phi_1$ | | $\Phi_2$ | | $\Phi_3$ | | $\Phi_4$ | | $\Phi_5$ | | $\Phi_6$ | |
|---|---|---|---|---|---|---|---|---|---|---|---|---|---|
| | $\mathrm{I_B}$ | $\mathrm{I_B}$ | $\mathrm{I_B^{corr}}$ | $\mathrm{I_B}$ | $\mathrm{I_B^{corr}}$ | $\mathrm{I_B}$ | $\mathrm{I_B^{corr}}$ | $\mathrm{I_B}$ | $\mathrm{I_B^{corr}}$ | $\mathrm{I_B}$ | $\mathrm{I_B^{corr}}$ | $\mathrm{I_B}$ | $\mathrm{I_B^{corr}}$ |
| BA5 | 0.40 | 2.24 | 2.93 | 6.81 | 12.32 | 22.4 | 39.5 | 54.4 | 100.0 | 171. | 268. | 263. | 490. |
| BC5 | 0.046 | 2.03 | 2.79 | 6.78 | 11.95 | 18.0 | 31.8 | 63.4 | 103.5 | 170. | 264. | 293. | 503. |
| BD5 | 0.47 | 2.69 | 3.53 | 5.28 | 9.83 | 15.7 | 28.3 | 46.9 | 78.2 | 125. | 207. | 289. | 484. |
| BE5 | 0.186 | 2.37 | 3.20 | 4.81 | 8.73 | 14.8 | 26.2 | 57.5 | 93.2 | 169. | 275. | 320. | 524. |

Table 5
The bulk current ($\mathrm{I_B}$) was measured before and after each irradiation step. The corrected bulk current ($\mathrm{I_B^{corr}}$) takes into account the partial annealing of the current. For each step the current due to the previous irradiations was calculated and subtracted from $\mathrm{I_B}$. Then the measurement was extrapolated to the day of the irradiaton (day 0). The extrapolations were done with Eq. (10), assuming 3 components and the parameters: $\mathrm{g_1} = 26\%,\ \tau_1 = 1.27\ \mathrm{d},\ \mathrm{g_2} = 26\%,\ \tau_2 = 7\ \mathrm{d},\ \mathrm{g_3} = 48\%,\ \tau_3 = 300\ \mathrm{d}$. Then for each step the cumulative current due to all the irradiations was added in $\mathrm{I_B^{corr}}$.
The very fast components of the decay are not considered because they are assumed not to be important for this study, the first and the second decays are taken from the literature on diodes (see Table 2) and the last component is an assumption based on the measurements in Section 5.6.
The currents are expressed in nA.

### 5.3. Gain

Notwithstanding the very complicated inner structure of the APD, the gain of the device does not change after irradiation in the region M>1. Only an unimportant change for the low voltage region was observed (it should be noted that only APD's with $SiO_2$ front window were irradiated). This can clearly be seen in Figure 11 where the ratio of the gain for the APD BC-17 (not irradiated) and BC5 (after $4 \cdot 10^{13}$neutrons/cm$^2$) was reported for low voltage. The gain is the same for high bias, but there is a drop of gain at low bias. This can be explained by the creation of a charged layer just beyond the surface of the APD which does not allow photoelectrons to be injected in the gain region. Above a given voltage this layer disappears and the photoelectrons can pass through. In order to calculate the gain of a heavily irradiated APD it is not correct to take the illuminated current at 10 V as a reference. The fit to the data was performed with the function:

$$\mathrm{f(V)} = 1 - \mathrm{a} \cdot e^{-\mathrm{V/b}} \quad \text{where } \mathrm{a} = 0.293 \text{ and } \mathrm{b} = 14.5\ \mathrm{V} \tag{12}$$

and a bias of 40 V was chosen as a reference for gain calculations.

This effect is not important for what concerns the application of these devices in CMS, because higher gains will be used. On the other hand, it must be taken into account for the measurement of the quantum efficiency which is usually done at 10 V.

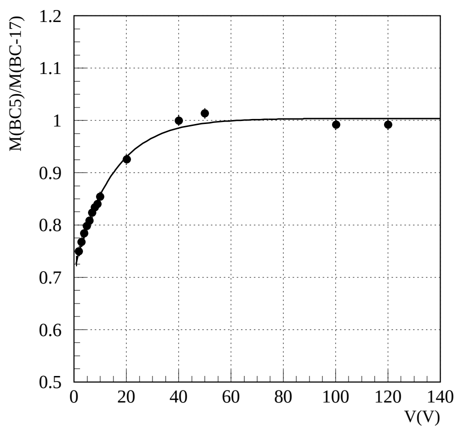


Figure 11. Ratio between the gain of the APD BC5 (after $4 \cdot 10^{13}$n/cm$^2$) and APD BC-17 (not irradiated). The gain was calculated as the ratio of the signal at a given bias and at a bias of 40 V.

### 5.4. Quantum efficiency

Only APD's with the front window of $SiO_2$ were irradiated. Figure 12 reports the quantum efficiency of the APD BC-17 (non irradiated) and BC5 (after $4 \cdot 10^{13}$n/cm$^2$). A drop in the quantum efficiency of about 10 % at 480 nm is observed.

### 5.5. Temperature dependence of the Dark Current after Irradiation

The temperature dependence of the dark current was measured after irradiations with different doses of neutrons. The bulk current contribution to the total dark current was evaluated from a fit, of the same type of the one shown in Figure 3. Then the bulk current dependence on the temperature (see Figure 13) was fitted with Eq. (11), where $\mathcal{E}_\mathrm{T}$ is the energy of the defects created by the neutrons, and is found to be around 0.6÷0.7 eV.

After the irradiations the bulk current contribution to the dark current dominates.

### 5.6. Room temperature annealing

Figure 14 shows the recovery of the dark current of the APD type BC, prototype # 24, which we have followed carefully for more than three months.

The measurements start after at least 2 days from the irradiation, because of safety reasons. With respect to Eq. (10) and Table 2, if the recovery is similar to the one of common diodes, there is no sensitivity to the very short

| APD | $\alpha(10^{-17}$A/cm) | $\alpha(10^{-17}$A/cm) (2 days) |
|---|---|---|
| BA5 | 15.6±1.6 | 11.3±1.2 |
| BC5 | 15.6±1.3 | 11.3±0.9 |
| BD5 | 13.6±1.2 | 9.9±0.9 |
| BE5 | 14.9±1.2 | 10.8±0.9 |
| BC-24 | 17.2±2.6 | 12.5±1.9 |
| BC-26 | 20.3±3.0 | 14.7±2.2 |

Table 6

Values of the parameter $\alpha$ in Eq. (9) estimated from a fit to the values of the current $I_B^{corr}$. The first value was calculated assuming the recovery as in Table 5 and extrapolating to the day of the irradiation. (This extrapolation is not realistic because it does not take into account the very fast components of the recovery, see Table 2, it must be considered as a reference point only). The second value is the estimate of the value of $\alpha$ two days after the irradiation. (According to the recovery parameters assumed, it is equal to the first value times a factor 0.726).

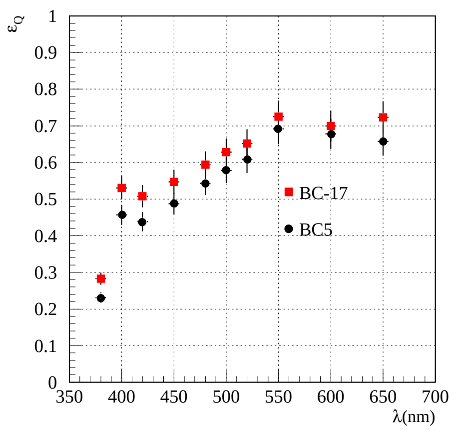


Figure 12. Quantum efficiency versus wavelenght for the APD BC5 (after $4 \cdot 10^{13}$n/cm$^2$) and APD BC-17 (not irradiated). The measurements were done at 24$^o$C.

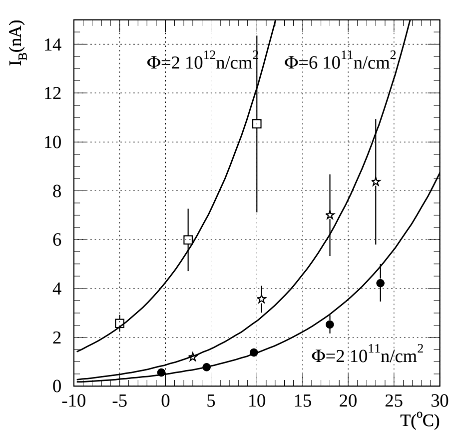


Figure 13. Bulk current dependence of the temperature after irradiation. The various neutron doses are indicated in the plot. The fit to the data is performed using Eq. (11).

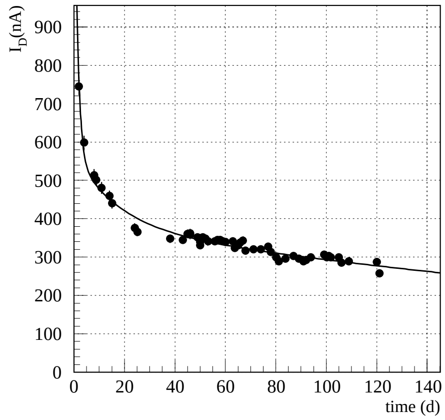


Figure 14. Room temperature annealing of the APD BC-24. This APD was irradiated with a dose of $1.4 \cdot 10^{12}$ n/cm$^2$. After the irradiation it was kept at room temperature under a bias of 180 V, corresponding to a gain of 42. The current in the figure is the total dark current measured for this bias.

components, the sensitivity to the 1.3 days component is marginal, while the mid and long term components can be precisely detected.

The data were fitted with three exponentials, fixing the first one to 1.3 days. The parameters of the fits for the various diodes are reported in Table 7. The behaviour of the dark current on the month scale confirms the measurements done on diodes, in fact the second exponential has a lifetime of the order of 1 week. But there is an indication that there is a further component of the annealing, which is not observed in the recovery of the common diodes. The lifetime of this third component is very long, of the order of 200÷300 days.

However a longer time is needed to understand if there is some component which does not recover at all like for the commercial diodes or if the recovery will be complete. These APD's are new devices and the doping profile is different from the one of the conventional diodes used in the measurements summarized in Section 1. So a stronger recovery with respect to diodes is well possible. As it will be shown in Section 6, even a very long component of the decay (of the order of 1 or 2 years) could help to reduce the noise to an acceptable level and it is then important to follow the evolution of the recovery for long time. Careful measurements on the type of defects induced by the radiation (with TSC or DLTS) could help to deeper understand the dynamics of the recovery and differences with commercial diodes.

In Figure 15 we compare the short term annealing rates of the APD BC-24 and BC-26 irradiated respectively to 1.4 and $4{\cdot}10^{12}$n/cm$^2$. To perform this comparison the dark currents were normalized to the value measured after 15 days, in order to avoid the possible instability due to the very fast components. From a comparison of the annealing rates in Table 7 we can see that the decay times do not depend on the doses.

Furthermore the annealing does not depend on wether or not the detector was kept under bias during the recovery. APD BC-24 was permanently under bias during the recovery while BC5 was not. Unfortunately BC5 was irradiated in several steps and a partial annealing took place during the irradiation. To see that the recovery does not depend on the bias, it is possible to compare the bulk current reached after 45 days from the last irradiation by BC5 (163 nA) and BC-24 (8.2 nA) and the current we would expect on the day of the irradiation for BC5 (503 nA) and BC-24 (28.7 nA). The ratio is (0.32±0.04) for BC5 and (0.29±0.02) for BC-24, in quite good agreement between themselves.

### 5.7. Additive property of the defects

Measurements and models existing on diodes show that the current is due to the various defects induced in the silicon lattice by the irradiation. Each defect has a given probability to appear and it is important to verify the additive property of the current generated by them. APD # 26 (BC type) was irradiated to $4{\cdot}10^{12}$n/cm$^2$. Then after about 50 days, when the recovery of the short components had taken place, it was irradiated again to half of the previous dose. The current after the second irradiation gives a value in good agreement with the sum of the residual current before the second irradiaton (1200 nA) plus the expected contribution of the new irradiation (1250 nA) (one half of the current due to the first irradiation). The recovery can be described by the usual sum of exponentials, whose parameters are given in Table 7. Different fitting techniques were tried and they give consistent results.

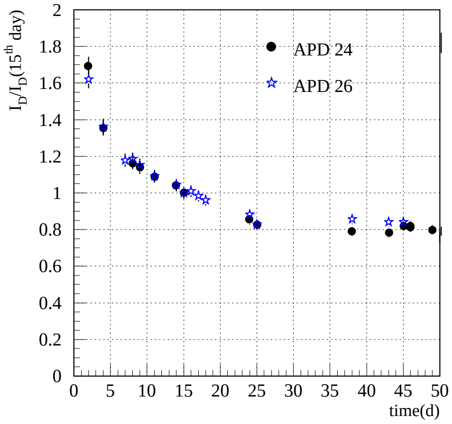


Figure 15. Room temperature annealing of the APD BC-24 and BC-26. The first was irradiated to $1.4 \cdot 10^{12}$ n/cm$^2$, while the second to $4 \cdot 10^{12}$ n/cm$^2$. The currents are divided by the measurement of the 15$^{\text{th}}$ day.

| APD | $\Phi(10^{12}$n/cm$^2)$ | Fit | $g_1$ | $\tau_1$ (d) | $g_2$ | $\tau_2$ (d) | $g_3$ | $\tau_3$ (d) | rec. hist. |
|---|---|---|---|---|---|---|---|---|---|
| BC-24 | 1.4 | e+e+e | 0.387 | 1.27 (fixed) | 0.271 | (8.4±1.0) | 0.342 | (325±50) | U.B. T∼20$^o$C |
| BC-26 | 4 | e+e+c | 0.348 | 1.27 (fixed) | 0.312 | (10.5±1.1) | 0.340 | $\infty$ (fixed) | U.B. T∼20$^o$C |
| BC-26 | 2 | e+e+c | 0.048 | 1.27 (fixed) | 0.336 | (21±10) | 0.616 | $\infty$ (fixed) | U.B. T∼20$^o$C |
| BC-25 | 0.49 | e+c | 0.204 | (4.1±1.4) | 0.796 | $\infty$ (fixed) | – | – | U.B. T∼0$^o$C |
| BC-25 | 0.49 | e+c | 0.354 | (5.3±0.7) | 0.443 | $\infty$ (fixed) | – | – | U.B. T∼20$^o$C |

Table 7
For each APD the Table shows the dose received, the type of fit used to reproduce the annealing behaviour and the estimated parameters, the recovery history followed by the APD.
(U.B. = under bias, e = exponential, c = constant)

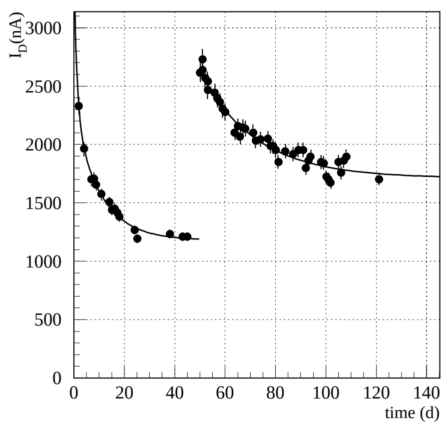


Figure 16. Room temperature annealing of the APD BC-26 after the first and second irradiation. The first dose was $4 \cdot 10^{12}$ n/cm$^2$, while the second was $2 \cdot 10^{12}$ n/cm$^2$.
The current is measured for a bias of 180 V, corresponding to a gain of 42.

Figure 17 shows a comparison between the annealing of the APD BC-26 after the first and the second irradiation (once subtracted the constant level due to the first and rescaled). The two curves are in quite good agreement within the errors.

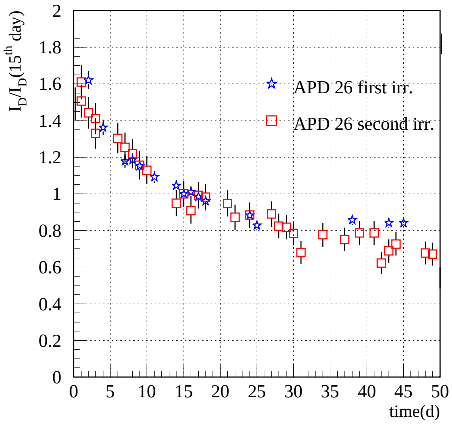


Figure 17. Room temperature annealing of the APD BC-26 after the first and second irradiation. The first dose was $4 \cdot 10^{12}$ n/cm$^2$, while the second was $2 \cdot 10^{12}$ n/cm$^2$. The second irradiation is subtracted of the residual current due to the first irradiation (1200 nA). The currents are divided by the measurement of the 15$^{\rm th}$ day.

### 5.8. Temperature dependence of the annealing

#### 5.8.1. Low temperature behaviour

APD BA5 was irradiated in six steps up to the dose of $4{\cdot}10^{13}$n/cm$^2$. Then (see Figure 18(a)) it was held in a refrigerator at about zero degrees from the sixth day after irradiation for about 45 days. During this time no significant recovery was observed. Thus it was held at room temperature and the recovery showed up as expected.

The same procedure (see Figure 18 (b)) was repeated on another APD (type BC, protoype # 25). This time the APD was held in a refrigerator directly after irradiation. It showed a relatively fast but not important recovery with a lifetime of 3.5 days and, after, quite stable conditions. (The reason why this fast component was not observed in BA5 resides in the fact that it was held in a refrigerator only six days after irradiation.) After 40 days the APD BC-25 was taken out of the refrigerator and its annealing started again.

## 6. Simulation of the damage and recovery dynamics in CMS

From Eq. (2) it is clear that the bulk current term in the noise will be the dominant term, after long time exposure to the radiation in CMS. Then the electronic noise can be approximated as:

$$\sigma(\mathrm{MeV}) \simeq \sqrt{\mathrm{k} \cdot \mathrm{I_B F}\tau}\frac{1}{\mathrm{N_{pe}}} \times 3 \qquad (13)$$

where the factor 3 takes care of the incoherent noise summed over a matrix of $3 \times 3$ crystals. Assumed values for the parameters in Eq.(13) are:

$$\mathrm{F} = 2,\;\; \mathrm{M} = 50,\;\; \tau = 30\,\mathrm{ns},\;\; \mathrm{N_{pe}} = 2.38\,\mathrm{p.e./MeV}\;\; [12] \text{ and } \mathrm{k} = 11.5\,\mathrm{nA^{-1}ns^{-1}}\;\; [2], \qquad (14)$$

were k is a constant depending on amplifier characteristics and the number of photoelectrons per MeV represents a conservative value, measured in 1995 test-beam on an old batch of crystals.

A tentative schedule of LHC estimates 10 years of data taking with 180 days of run per year divided in three periods of 60 days each and separated by 10 days of pause. In the remaining part of the year, a long winter shutdown takes place.

In [13] the author estimates a rate of $\frac{d\Phi}{dt}$ $=0.11{\cdot}10^{11}$ n/cm$^2$/day, which gives a total dose of $2{\cdot}10^{13}$ n/cm$^2$ in 10 years. According to Eq. (9), the dark current increases linearly with the accumulated dose. If no recovery takes

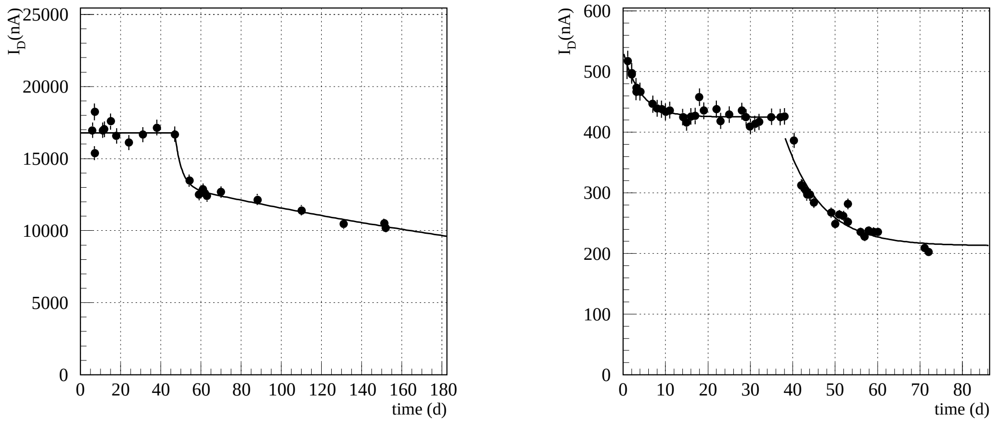


(a) BA5 (b) BC-25

Figure 18. (a) Low temperature annealing of the APD BA5 after $4 \cdot 10^{13}$ n/cm$^2$. (b) Low temperature annealing of the APD BC-25 after $4.9 \cdot 10^{11}$ n/cm$^2$. After about 40÷50 days they were stored at room temperature and the recovery started again. The current was measured for a gain of about 50 (that is 193 V) for BA5 and 42 (bias=180 V) for BC-25. The currents are rescaled at 18$^o$C. In the first case BA5 was held at low temperature, but measured at room temperature, while BC-25 was held and measured at low temperature.

place, assuming $\alpha = 9 \cdot 10^{-17}$A/cm for the APD's, an estimate of the bulk current and the noise is shown in Figure 19, curve ($a$). This is a very pessimistic case and it is not realistic, because there is evidence for a recovery of the dark current.

A simple model for the damage and recovery of the current can be formulated taking care of the LHC running schedule. Assuming that several defects are created independently in the silicon bulk, the current induced by the irradiation due to a single trap type $i$ increases proportionally to the dose $\Phi$ and the coefficient $\alpha_\mathrm{i}$:

$$\mathrm{dI}^{(\mathrm{irr})}_{\mathrm{trap\ i}} = \alpha_\mathrm{i} \mathrm{V} \mathrm{d}\Phi. \tag{15}$$

The total current is the sum of the various contributions given by each type of defect:

$$\mathrm{I}^{(\mathrm{irr})} = \sum_\mathrm{i} \mathrm{I}^{(\mathrm{irr})}_{\mathrm{trap\ i}}. \tag{16}$$

The trap due to each defect recovers with its proper lifetime $\tau_\mathrm{i}$:

$$\mathrm{dI}^{(\mathrm{rec})}_{\mathrm{trap\ i}} = -\frac{\mathrm{dt}}{\tau_\mathrm{i}}. \tag{17}$$

For each trap, the evolution in time of the current is governed by the equation:

$$\mathrm{dI}_{\mathrm{trap\ i}} = \mathrm{dI}^{(\mathrm{irr})}_{\mathrm{trap\ i}} + \mathrm{dI}^{(\mathrm{rec})}_{\mathrm{trap\ i}} = \alpha_\mathrm{i} \mathrm{V} \mathrm{d}\Phi - \frac{\mathrm{dt}}{\tau_\mathrm{i}}, \tag{18}$$

where:

$$\begin{cases} \mathrm{d}\Phi = 0 & \text{(shutdown or pause)} \\ \mathrm{d}\Phi = \frac{\mathrm{d}\Phi}{\mathrm{dt}} \cdot \mathrm{dt} & \text{(data-taking)} \end{cases} \tag{19}$$

Thus the behaviour of the current at time t after the last change of running mode at $\mathrm{t_o}$ is:

$$\mathrm{I}_{\mathrm{trap\ i}}(\mathrm{t}) = \begin{cases} \mathrm{I}_{\mathrm{trap\ i}}(\mathrm{t_o}) \mathrm{e}^{-\mathrm{t}/\tau_\mathrm{i}} & \text{(shutdown)} \\ (\mathrm{I}_{\mathrm{trap\ i}}(\mathrm{t_o}) - \alpha_\mathrm{i} \mathrm{V} \frac{\mathrm{d}\Phi}{\mathrm{dt}} \tau_\mathrm{i}) \mathrm{e}^{-\mathrm{t}/\tau_\mathrm{i}} + \alpha_\mathrm{i} \mathrm{V} \frac{\mathrm{d}\Phi}{\mathrm{dt}} \tau_\mathrm{i} \longrightarrow \alpha_\mathrm{i} \mathrm{V} \frac{\mathrm{d}\Phi}{\mathrm{dt}} \tau_\mathrm{i}\ (\mathrm{t} >> \tau_\mathrm{i}) & \text{(data-taking).} \end{cases} \tag{20}$$

Figure 19 shows 3 possibilities:
($a$) one trap with no recovery ($\tau_1 = \infty$, $\alpha_1 = 9 \cdot 10^{-17}$A/cm/n),

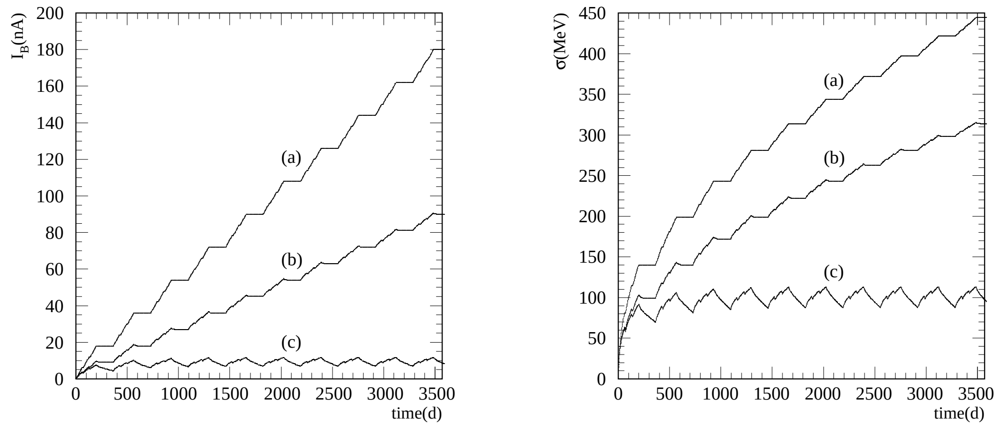


(a) (b)

Figure 19. Bulk current (a) and electronic noise given by a 3×3 matrix (b) estimate in CMS. See the text for details on the curves.

($b$) two traps ($\tau_1 = 15$ days, $\tau_2 = \infty$, $\alpha_1 = \alpha_2 = 4.5 \cdot 10^{-17}$A/cm/n),
($c$) two traps ($\tau_1 = 15$ days, $\tau_2 = 1$ year, $\alpha_1 = \alpha_2 = 4.5 \cdot 10^{-17}$A/cm/n).
It's clear that it is very important to understand wether or not there is a long component of the annealing. Indeed from Eq. (20) even a component with a very long lifetime gives a contribution equivalent at most to an exposure equal to its proper lifetime and not to the effective time of exposure.

### 6.1. Conclusions

The characteristics which were investigated for this batch of APD's before irradiation are progressively approaching the CMS requirements. The dark current before irradiation is very low, especially for the APD BA-N, with the $Si_3N_4$ window. The quantum efficiency for this APD is also higher than the one of the APD with the $SiO_2$ window, as expected from the different reflectance of the materials. The temperature dependence of the dark current is in good agreement with the theory.

The dark current induced by the irradiation shows a linear behaviour with the administered dose and the $\alpha$ parameter is compatible with the measurements performed on diodes, assuming a thickness $\mathrm{d_{eff}} = 5\mu\mathrm{m}$.

For what concerns the recovery:

- The time dependence of the recovery for these devices shows a behaviour similar to the one of diodes for what concerns the fast components.
- Measurements give indication for a long decay-time component.
- No difference is observed in the recovery between APD's kept under bias or not during the recovery.
- No difference is observed in the recovery time constants of APD's irradiated at different doses and the defects seem to cumulate linearly, as expected.
- Measurements show evidence for a strong reduction of the recovery at low temperature.

We assume a model for the damage and recovery of the dark current during the operation of CMS. From this model it appears that it is very important to understand wether or not a long component of the annealing is present.

## 7. Acknowledgements

Clarifying discussions with J.L. Faure, Y. Moussienko and D. Renker are acknowledged.

**REFERENCES**


1. *CMS Technical Proposal*, CERN/LHCC 94-38, (1994).
2. Y. Benhammou, P. Depasse, M. Goyot, B. Ille, E. Linard, F. Martin, Y. Musienko, D. Si Mohand, *Investigation of Avalanche Photodiodes*, CMS TN/96-052.
3. S. Baccaro, B. Borgia, F. Cavallari, I. Dafinei, M. Diemoz, A. Festinesi, E. Longo, M. Montecchi, G. Organtini, A. Piegari, *Detection of photons generated in $PbWO_4$ scintillator crystals*, CMS note in preparation.
4. S. M. Sze, *Physics of semiconductor devices*. Wiley and Sons (New York) 1981.
5. E. Borchi, M. Bruzzi, *Radiation damage in silicon detectors*, Riv. del N. Cim., vol.17, N. 11 (1994).
6. Nucl. Instr. and Meth. A377 Nos. 2,3 (1996), section II *Radiation damage*, Proceedings of the Seventh European Symposium on Semiconductor Detectors, Schlo$\beta$ Elman, Bavaria, Germany, May 7-10 1995.
7. M. Huhtinen and P. Aarnio, *Pion induced displacement damage in silicon devices*, Nucl. Instr. and Meth. A335 (1993) 580.
8. G. Hall, *Radiation resistance of semiconductor detectors and associated electronics*, Proceedings of the LHC Workshop, Aachen, October 1990. CERN 90-10, vol. 3, 693.
9. M. Bosetti, C. Furetta, C. Leroy, S. Pensotti, P.G. Rancoita, M. Rattaggi, M. Redaelli, M. Rizzatti, A. Seidman, G. Terzi, *Effect on charge collection and structure of n-type silicon detectors irradiated with large fluences of fast neutrons*, Nucl. Instr. and Meth. A 343 (1994) 435.
10. S. Baccaro and A. Festinesi, *Gamma and neutron irradiation facilities at ENEA-Casaccia Center* (Roma), CMS-TN/95-192.
11. F. Cavallari, *Progress on Avalanche Photodiodes as photon detectors for $PbWO_4$ crystals in the CMS experiment*, talk presented at th 5th International Conference on Advanced Technology and Particle Physics, Villa Olmo (Como-Italy) 1996, to be published in Nucl. Phys. B (Proc Suppl.).
12. Y.Benhammou, P. Depasse, H. El Mamouni, M. Goyot, B. Ille, P. Lebrun, Y. Musienko, D. Si Mohand, *Beam test results with fast preamplifiers associated to APDs readout of $PbWO_4$ crystal*, CMS TN/95-122.
13. M. Huhtinen, *Radiation environment simulation for the CMS detector*, CMS-TN/95-198, presented at the Second Workshop on Simulating Radiation Environments, CERN, Geneva, Switzerland, 9-11 October 1995.